Crosslinked gelatin nanofibres: Preparation, characterisation and in vitro studies using glial-like cells

Crosslinked gelatin nanofibres: preparation, characterization and *in vitro* studies using glial-like cells

C. Tonda-Turo[1], E. Cipriani[2], S. Gnavi[3], V. Chiono[1], C. Mattu[1], P. Gentile[1], I. Perroteau[3], M. Zanetti[2] and G. Ciardelli[1,4]

1 Politecnico di Torino, Department of Mechanical and Aerospace Engineering, Politecnico di Torino , Corso Duca degli Abruzzi 24, Torino, Italy

2 Nanostructured Interfaces and Surfaces (NIS) Centre of Excellence, Department of Chemistry IFM, Università di Torino, Via P. Giuria 7, Torino, Italy

3 Department Of Human and Animal Biology, Università di Torino, Via Accademia Albertina, 23, Torino, Italy

4 CNR-IPCF UOS Pisa Via Moruzzi, 1, 56124 Pisa

Corrisponding Author: Prof. Gianluca Ciardelli
gianluca.ciardelli@polito.it
phone:+39 011 0906919
fax:+39 011 0906999

Abstract. Gelatin (GL) nanofibrous matrices mimicking the complex biological structure of the natural extracellular matrix (ECM) were prepared from aqueous solutions by electrospinning technique. GL nanofibres with a diameter size of around 300 nm were obtained optimizing the process and solution parameters. To increase the GL stability in aqueous environment γ-glycidoxypropyltrimethoxysilane (GPTMS) was used as GL crosslinker. GPTMS crosslinking did not modify the nanofibrous matrix morphology: fibre diameter and membrane pores size were 327±45 nm and 1.64±0.37 μm, respectively. The produced GPTMS crosslinked GL nanofibres (GL/GPTMS_NF) were found to support the *in vitro* adhesion, proliferation and survival of neonatal olfactory bulb ensheating cells (NOBECs).

Keywords: electrospinning, gelatin, nanofibres, aqueous solution, glial cells

1. Introduction

Appropriate fibrous substrates, functioning as a temporary extracellular matrix (ECM), can be easily prepared by electrospinning, which allows the obtainment of random or aligned fibrous matrices with fibre diameters ranging from tens of nanometres to several microns by tuning processing parameters [1-2]. Fibre orientation and size can significantly influence the morphology, proliferation rate, phenotype, and function of cell types [3-6]. A wide range of polymers have been used to produce electrospun fibres [7-12]. Among them, natural polymers, such as proteins (gelatin, collagen and silk fibroin) and polysaccharides (chitosan, hyaluronic acid and cellulose) are functionally superior to non- informational synthetic polymers: as components of natural ECM or having a similar composition to ECM components, natural polymers provide chemical cues which facilitate cell attachment [13].

However, processing conditions for proteins have to be carefully selected as the use of high temperatures and organic solvents may cause protein denaturation [14]. On the other hand, polysaccharide electrospinning is also critical due to the relative high viscosity , which limits the spinnability [15].

An analysis of the state-of-the-art on protein and polysaccharide electrospinning showed that organic solvents have been generally used for processing [15-17]. Gelatin (GL) is a commercially available biomaterial that has widely used in biomedical engineering due to its similarity to the more expensive collagen adhesive protein [18-20]. GL has been successfully electrospun by using organic solvent such as 2,2,2-trifluorothanol [21], acetic acid [22], hexafluoroisopropanol [23] and formic acid [24]. Although in such studies, GL nanofibres with regular morphology have been obtained, the use of organic or acidic solvents for GL processing includes several drawbacks: (i) it can induce GL denaturation and degradation; (ii) traces of un-removed solvent residues may induce toxic effects *in vivo*; (iii) processing is expensive and not environmentally friendly. In addition, electrospun GL nanofibres should resist dissolution and degradation *in vivo* for the required time for cell adhesion, proliferation and deposition of natural ECM. As GL is water-soluble, crosslinking is required. Typical GL crosslinkers are aldehydes (formaldehyde, glutaraldehyde, glyceraldehyde)[25], carbodiimides [26], and enzymatically or naturally derived crosslinking agents[19-20].

The above mentionated crosslinkers require a post-electrospinning crosslinking step, based on incubation of GL nanofibres in suitable crosslinker containing water-based media for an appropriate time [27-29]. During

the crosslinking step, morphology of electrospun GL nanofibres can be severely altered, due to fibre swelling and partial or complete dissolution.

On the other hand, physical methods for GL crosslinking, including UV irradiation [30] or dehydrothermal treatment [31], do not require an incubation step in water based media, however they generally result in a low crosslinking degree, with consequent high swelling and rapid dissolution of GL nanofibres when implanted *in vivo*.

In this work, the above criticisms on the production of stable electrospun GL nanofibres are solved through using water as solvent for GL electrospinning: water is not toxic, its use avoids the risk of protein denaturation during processing and it is an environmentally friendly and cheap solvent. In general, electrospinning of aqueous GL solutions at room temperature cannot be performed due to the formation of a three-dimensional interconnected network of GL chains below the sol-gel transition temperature (~ 30°C). On the other hand, GL electrospinning from water solutions is possible at temperatures of around 50°C as previously shown by few authors [29-32]. Respect to previous literature dealing with GL electrospinning from water solutions, one of the main innovative contributions of the present work derives from the accurate analysis of a series of experimental parameters for GL electrospinning, with the aim to select optimal processing conditions to obtain regular fibrous matrices with appropriate pore size and fibre diameters. In detail, electrospinning process parameters were tuned to obtain GL porous matrices with a pore size of around 1-2 μm (suitable for nutrients permeation) and composed of fibres characterised by a diameter of around 300 nm (suitable for glial cells adhesion and proliferation) [4].

Previous studies on GL electrospinning from aqueous solutions [29] have proposed GL crosslinking as a separate second step after electrospinning. However, this post electrospinning processing may lead to an alteration of fibre morphology caused by GL swelling and partial dissolution during incubation in a crosslinker containing water medium. In the present work, an innovative crosslinking method for GL nanofibers was proposed based on the addition of the crosslinker into the GL water solutions before processing. To this purpose, a silane-coupling agent (γ-glycidoxypropyltrimethoxysilane, GPTMS), which has been reported previously to form biocompatible GPTMS crosslinked GL membranes [33], has been used. In the GPTMS crosslinking mechanism, the oxirane rings on the GPTMS molecules react with the

amino groups on the GL chains and hydrolysis of the trimethoxy groups on the GPTMS forms pendant silanol groups (Si-OH) through an acid catalyzed reaction (equation 1).

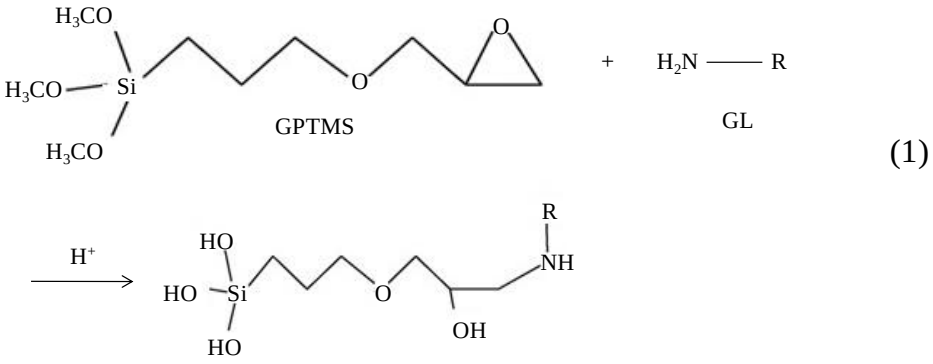

(1)

Then, Si-O-Si bonds are formed through the condensation of two Si-OH which occur mainly during solvent evaporation. The Si–O–Si linkages formed from condensation reactions provide inter-chain covalent bonds resulting in a crosslinked structure (equation 2) [34].

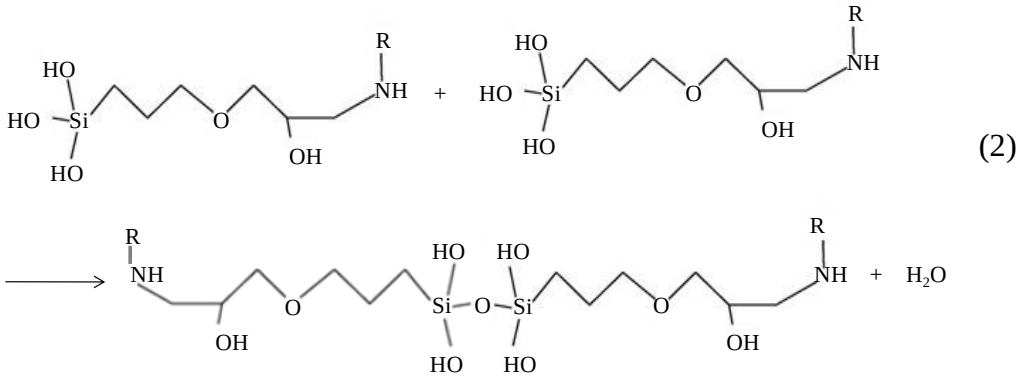

(2)

Unlike other GL crosslinkers which can be introduced into polymeric solutions before electrospinning (e.g. genipin) [28], the addition of GPTMS does not modify the viscosity of the GL water solution during processing, as the final step of GPTMS crosslinking (which is a condensation reaction) occurs during solvent evaporation, after that the fibres have been spun and collected.

The crosslinked nanofibres were characterized by scanning electron microscopy (SEM) for their morphology and pore size and by dissolution tests in phosphate buffered saline (PBS) for their water stability. *In vitro* cell tests using glial-like cells were performed on GPTMS crosslinked GL nanofibres (GL/GPTMS_NF). Neonatal olfactory bulb ensheating cells (NOBECs) were selected as the glial cell type to perform *in vitro* cell tests since, as compared to Schwann cells (SCs), they produce more trophic factors [35] and do not

express growth-inhibitory proteoglycans common to SCs [36]. Moreover, OECs increase axonal regrowth and Schwann cell-mediated peripheral nerve regeneration and functional repair after nerve injury in adult rats [37-38]. In the field of neural tissue engineering, fibrous matrices are particularly useful as they can be engineered to have high porosity, high surface-to-volume ratio, and high pore interconnectivity: these physical properties can promote adhesion and proliferation of glial cells. In this work, *in vitro* results were obtained showing the adhesion, proliferation and viability of NOBECs on the electrospun GL matrices. Moreover, NOBECs-GFP cultured on GL/GTPMS_NF revealed that cells were organized in cords and the cell bodies had an elongated appearance.

2. Materials and Methods

2.1. Sample preparation

2.1.1. Electrospinning procedure and parameters.

The electrospinning technique utilises an electric field generated by an applied voltage that subsequently introduces surface charges on the polymer solution. This induces the formation of a Taylor cone on the polymeric solution droplet at the tip of the spinneret. Whenever the electric potential that is formed at the droplet surface exceeds a critical value, the electrostatic forces overcome the solution surface tension to initiate a polymeric jet stream. Nanofibres can then be drawn from the polymeric jet stream, and collected on the grounded collector as the solvent evaporates. The morphology, the size and the shape of the electrospun fibres can be controlled by varying the process and solution parameters [39]. The electrospinning system used for fibre preparation was assembled inside a vented hood equipped with an extraction system for solvent vapours. A structure of expanded polyurethane was set up inside the hood. This structure functions as an isothermal chamber (it contains two electric lamps which raise the temperature up to a maximum of 80° C). The electrospinning system consisted of a high voltage source (placed outside the hood so as not to interfere with the electric field), an electrode, a syringe without the needle, a volumetric pump, a support and a collector.

The high voltage generator used was the PS/EL30R01.5-22 Glassman High Voltage, providing a voltage of 0 to 30 kV and a current of 0 to 1.5 mA with reversible polarity. The volumetric pump (KDS210 of KD Scientific) was set to have a flow rate of 8 µl min^{-1} to 15 µl min^{-1}. The syringe was coupled to a teflon

capillary, cut at one end and connected to a metal adapter in contact with the electrode to transmit the electrical potential to the solution. The capillary was mounted on polymeric support material to avoid the dispersion of dangerous electrical charges and interference with the electric field.

The support was mobile, so that the distance between nozzle and collector could be varied (the maximum possible distance between nozzle and collector was 19 cm).

The collector was composed of aluminium sheets of about 1.5 mm thickness, bolted onto a support and connected to a cable for grounding. A nozzle-collector system with the nozzle parallel to the support base was used to prepare the nanofibrous matrices. This geometry avoided the deposition of drops of solvent on the samples ensuring uniform samples preparation.

2.1.2. Solution preparation.

GL (type A from porcine skin) and GPTMS were supplied by Aldrich. GL was dissolved in demineralised water at 50°C to obtain the desired solution concentration. Nanofibrous scaffolds were prepared by the electrospinning using a flat aluminium plate to collect randomly oriented nanofibres. Uncrosslinked scaffolds were prepared from the GL solutions as reported in table 1 which collects the spinning parameters and the sample codes. The solution was spinnable in the following conditions: at a temperature of 50°C, with solution concentrations of 8% to 20% (w v^{-1}), at a flow rate of 10 µl min^{-1} to 18 µl min^{-1} and with nozzle-collector distance of 7 cm to 19 cm. The applied voltage was maintained at 30kV for the samples preparation.

Table 1. Spinning parameters used for GL nanofibres preparation.

Sample code	**Solution concentration (% w·v^{-1})**	**Flow rate (µl·min^{-1})**	**Nozzle-collector distance (cm)**
GL1_NF	**8**	10	15
GL2_NF	**10**	10	15
GL3_NF	**12**	10	15
GL4_NF	**15**	10	15
GL5_NF	**18**	10	15
GL6_NF	**20**	10	15

GL7_NF	15	**8**	15
GL4_NF	15	**10**	15
GL8_NF	15	**12**	15
GL9_NF	15	**15**	15
GL10_NF	15	10	**7**
GL11_NF	15	10	**10**
GL4_NF	15	10	**15**
GL12_NF	15	10	**19**

The GPTMS crosslinked GL nanofibres (GL/GPTMS_NF) were prepared from GL/GPTMS solutions, adding an appropriate amount of GPTMS to the GL solution and mixing for one hour before spinning. The amount of GPTMS was calculated with respect to the molar concentration of amino groups in hydroxylysine, lysine and arginine residues of GL to obtain a molar ratio of 2:1 between the GL amino groups and the GPTMS molecules as described by Liu et al. [40] (92 µl of GPTMS were added per GL gram).

2.1.3. Cell culture and fibre sterilization.

In vitro cell tests were performed using neonatal olfactory ensheating cells (NOBECs). The NOBEC cell line was derived from primary cells dissociated from the neonatal rat olfactory bulb and immortalized by retroviral transduction of the SV40 large T antigen [41].

NOBECs and NOBECs which express green fluorescent protein (NOBECs-GFP) were grown in a monolayer at 37°C in a humidified atmosphere of 5% $CO_2 \cdot air^{-1}$, in Dulbecco's modified Eagle's medium (DMEM) supplemented with 100 units ml^{-1} penicillin 0.1 mg ml^{-1} streptomycin, 1 mM sodium pyruvate, 2 mM L-glutamine, and 10% heat-inactivated fetal bovine serum (FBS, Invitrogen).

Before cell seeding, material samples were sterilized by exposition to UV irradiation for 30 minutes and then incubated with DMEM overnight. For the *in vitro* cell test, GL/GPTMS_NF samples were inserted into 24-multiwell plates containing coverslips and CellCrowns (Scaffdex) were used to avoid floating of the samples.

2.2. Sample Characterization

2.2.1. Morphology and pore size.

The morphology of the electrospun matrices was analysed under a scanning electron microscope (SEM Philips 525M) at an accelerate voltage of 15 kV. The SEM magnification (6000x) was selected to have a squared analisy fields of 50μm, allowing the analysis of the nanofibres distribution for all the prepared samples.

Before SEM analysis, samples were coated with silver using a sputter coater. The samples soaked in PBS were freeze-dried to remove remaining water. The pore and fibre diameters were quantified by analysing the SEM micrographs using the ImageJ software. Three images of three different zones of three samples were analyzed and the pore and fibre diameters were reported as average value ± standard deviation.

2.2.2. Fourier transform infrared-attenuated total reflectance spectroscopy (FTIR-ATR).

Chemical analysis of GL_NF and GL/GPTMS_NF was performed by ATR-FTIR spectroscopy over a range of 2000 cm^{-1}- 800 cm^{-1} using Perkin Elmer equipment (Spectrum 100 with UATR KRS5).

2.2.3. Dissolution tests.

The dissolution behaviour of GL/GPTMS_NF nanofibres was evaluated soaking weighted samples (W_0) in PBS for 1, 2, 4, 7, 10 and 14 days. At each time point, samples were removed from PBS and dried at 37 °C for 48 h in a vented oven. Then, samples were weighed again (W_d) and the dissolution percentage was calculated as:

$$\Delta W_d(\%)=((W_0-W_d)/W_0) \times 100 \quad (3)$$

For each experimental time, five samples were measured and the result was expressed as an average value ± standard deviation.

A qualitative analysis of the dissolution behaviour of GL/GPTMS_NF was performed by dipping the nanofibrous membranes into PBS at pH 7.4. For each sample, five rectangular nanofibrous membranes deposited on the rectangular metal collector (1 cm x 3 cm) were soaked in 5 ml of PBS and maintained at

37°C. After 6, 48 and 168 hours, samples were collected and dried. Morphology of nanofibres was analyzed by SEM.

2.2.4. In vitro cell test

Viability test: Adhesion and Proliferation assay

Adhesion assay.

To assess the ability of GL/GPTMS fibres to allow cell adhesion, NOBECs were seeded in DMEM containing 10% FBS, at a density of 1000 cells·cm^{-2} on both poly-L-lysine (Sigma) coated coverslips (control condition) and GL/GPTMS_NF. After 3 hours, the culture medium was removed, substrates with attached cells were rinsed with PBS with Ca^{2+} and Mg^{2+} and fixed by the addition of 4% paraformaldehyde solution (PAF, Sigma-Aldrich). After 20 minutes, the PAF was removed and samples were rinsed with PBS with Ca^{2+} and Mg^{2+} and then stained with 4, 6-diamidino-2-phenylindole (DAPI) diluted 1:1000 in PBS. DAPI is a fluorescent stain that binds strongly to DNA. When bound to double-stranded DNA, its absorption maximum is at 358 nm and its emission maximum is at 461 nm, and it appears blue/cyan. Cells were photographed by an Olympus IX50 microscope with a RS Photometrics camera. For each sample, four images were taken with at low magnification. The images were then acquired through Image Pro Plus and the number of adherent cells was counted with Image J. The experiment described above includes the use of 3 sets of plates. Each set includes 3 GL/GTPMS_NF matrices and 3 control poly-L-lysine coated coverslips. The counts obtained from assays were analyzed, averaged, and expressed as the number of adherent cells·mm^{-2} ± standard deviation.

Proliferation assay.

NOBECs were seeded at a concentration of 1000 cells·cm^{-2} on GL/GTPMS_NF and control coverslips in medium with DMEM containing 10% FBS. After 1, 3, 5, and 7 days, cells were fixed, stained, photographed and counted as described in the adhesion assay paragraph. For each time interval, 3 GL/GTPMS_NF matrices and 3 control poly-L-lysine coating coverslips were used and the experiments were repeated three times independently. Numbers of cells counted for each assays were analyzed, averaged, and expressed as number of cells ± standard deviation.

Apoptosis assay: DeadEnd Fluorimetric Tunel System.

NOBECs were plated in 0.5 ml of DMEM containing 10% FBS at a density of 1000 cells·cm^{-2} in 24-wells plates containing poly-L-lysine and GL/GTPMS_NF coated coverslips. After 3 hours of culture in DMEM 10% FBS, NOBEC cell were starved for 72 hours in a serum free medium. Positive control for biological apoptosis was performed on both poly-L-lysine and GL/GTPMS_NF coated coverslips by a 24 hours treatment with 100 μM cycloheximide. Cycloheximide (CHX) is an antibiotic produced by S. griseous. Its main biological activity is translation inhibition in eukaryotes resulting in cell growth arrest and apoptosis induction [42]. DNA strand breaks were stained with TUNEL (TdT-mediated dUTP Nick End Labeling) staining reagent according to the manufacturer's instructions (DeadEnd^{TM} Fluorimetric TUNEL System, Promega). Technical positive control reactions were performed on both poly-L-lysine and GL/GTPMS_NF coating coverslips using DNase I following the manufacturer's instructions. Technical negative control reactions were performed on both poly-L-lysine and GL/GTPMS_NF coated coverslips in a control incubation buffer without rTdT. Total nuclei were stained with 4',6-diamidino-2-phenylindole (DAPI; Sigma-Aldrich) 0.2 μg·ml^{-1} for 10 minutes at room temperature. The coverslips were mounted with fluoromount medium (Sigma Aldrich). Cells were photographed using an Olympus IX50 microscope with an RS Photometrics camera. For each sample, four images were taken at low magnification. The images were then acquired through Image Pro Plus and the number of apoptotic nuclei was counted using Image J. The experiment described above includes the use of 3 sets of plates. Each set includes 8 GL/GTPMS fibres and 8 control poly-L-lysine coated coverslips. The counts obtained from assays were analyzed and expressed as a percentage of apoptotic nuclei/total nuclei ± standard deviation.

Cell viability and cytotoxicity assay: 3-(4,5-dimethylthiazol-2-yl)-2,5-diphenyltetrazolium bromide (MTT) assay.

Potential biomaterial cytoxicity was evaluated by 3-(4,5-dimethylazol-2-yl)-2,5-diphenyltetrazolium bromide (MTT) assay. 2×10^4 NOBECs were plated in 0.2 ml of DMEM containing 10% FBS on GL/GTPMS_NF and control condition in a 48-well tissue culture plate. In order to quantify the cell number serial dilution were performed by plating 1×103, 2×103, 4×103, 8×103, 1.6×104, 3.2×104, 6.4×104 per well. After a 1, 3, 5 and

7 days incubation, 10 ul of MTT substrate (Sigma, 5 mg/ml in phosphate buffered saline) was added, and the cells were incubated at 37°C for 4 hours. Mitochondrial dehydrogenase in living cells converts the yellow water-soluble tetrazolium salt 3-(4, 5-dimethylthiazol-2-yl)-2, 5 –diphenyltetrazolium bromide into dark blue formazan crystals that are stored in the cytoplasm of the cells. Then, the MTT solution was removed, and cells were washed twice with 0.5 ml of phosphate-buffered saline solution. Dimethyl sulfoxide (DMSO; Sigma) was added to each well to dissolve the formazan. The plate was incubated at room temperature on a shaker for 30 minutes to enhance the dissolution of the formazan. A 100-µl aliquot from each well was transferred to a 96-well tissue culture plate. The spectrophotometric absorbance was measured at 570 nm wavelength, using DMSO as blank. Viability (%) was determined as (experimental group $A_{490\ nm}$/ control group $A_{490\ nm}$) × 100%. Each assay was performed in triplicate.

Actin cytoskeleton Staining.

Culture-insert StemCell (Ibidi, Cat. Nr 80409) were placed in a µ-dish (35 mm, high) glass bottom petri dish (Ibidi, Cat.Nr. 811156) covered with GL/GTPMS_NF or poly-L-lysine. NOBEC cells were counted and suspended at a density of 1×10^4 cells/ml and 10 ul were applied into each cell culture-insert well. After 24 hours of incubation, cells were fixed with paraformaldehyde for 20 minutes and washed twice with phosphate buffered solution (PBS, Sigma). Fixed cells were permeabilized with 0.1% Triton X-100 in 1X PBS for 5 minutes at room temperature and blocking solution (normal goat serum diluted 1:10 in 1X PBS, DAKO X0907) was applied for 1 hour at room temperature. F-actin was detected using TRITC conjugated phalloidin (diluted 1: 2000 in blocking solution; Millipore No.90228) by 1 hour incubation at room temperature following three washes step of 5 minutes each. Fluorescent images were acquired using a Nikon T-E microscope with a Plan Fluor 40× (Nikon) (numerical aperture (NA) = 0.45) and a Plan Fluor 40× (Nikon) (numerical aperture (NA) = 0.75).

Confocal microscopy.

In order to facilitate the observation of seeded cells, NOBECs-GFP were used. NOBECs-GFP were seeded on both GL/GTPMS fibres and poly-L-lysine coated coverslips at a concentration of 10^3 cells cm^{-2} in medium with DMEM containing 10% FBS. After 1 and 3 days, cells were fixed and nuclei were stained with DAPI (Sigma).

Confocal imaging was carried out with an LSM 510 confocal laser microscopy system (Zeiss, Jena, Germany), equipped with an inverted Axiovert 100M microscope. Confocal fluorescence images were acquired using a 20× Plan-NEOFLUAR objective (numerical aperture (NA) = 0.50). GFP fluorescence was excited at 488-nm, detected between 505 to 530 nm and visualized in green. DAPI was excited at 350-358 nm, detected between 510 to 550 nm and visualized in blue.

2.2.5 Statistics

Statistical analysis was carried out using SPSS software to execute single-factor analysis of variance test (ANOVA). A value of *$p<0.05$ and ***$p<0.01$ was considered statistically significant.

3. Results

3.1. Preliminary analysis of non-crosslinked GL nanofibres

The morphology, the size and the shape of the electrospun fibres can be controlled by varying the process and solution parameters. Figure 1 showed representative SEM micrographs of the samples prepared using different process and solution parameters.

The solution concentration range that allowed spinnability was from 8% to 20%; for concentration of less than 8% continuous nanofibres did not form during the electrospinning process while increasing the polymer concentration over 20% a too thick gel forms and the solution fail to be spun. Although GL nanofibres with a diameter of approximately 250 nm were obtained using solution with 8% concentration, both beads and droplets were also formed, reducing the uniformity of the electrospun fibres (figure 1 (a)). The bead formation phenomenon is well known and is related to solution viscosity, which varies with the solution concentration and affects the morphology of electrospun nanofibres. At low concentration, the viscosity of the solution is low, while the surface tension is relatively high. Therefore, the solution jet, which would form

nanofibres, cannot maintain its own shape at the end of tip due to high surface tension and tend to form small drops along the fibres. These effects cause the formation of beads instead of fibres, reducing the uniformity of the electrospun fibres.

The analysis of the influence of solution concentration on fibre morphology showed that for highly concentrated and viscous solutions, fibre diameters increased (figure 2(b)) from 243±98 nm for G1_NF to 523±104nm for G6_NF due to the higher GL weight percentage per volume of the solvent. Significant differences (*$p<0.05$) in fibres size were observed for low concentrations (8, 10, 12 %) against 20%. Moreover, for intermediate solution concentrations, the standard deviations of the fibre diameters were the lowest of all suggesting a more homogeneous fibres size distribution. Solution concentration also influenced the pore dimensions: no significant differences (*$p<0.05$) were observed for the mean pore size of all samples (figure 2c)), however the analysis of pore dimension distribution (figure 2(a)) showed the presence of pores with size in the range of 3-6 µm and 6-9 µm for solution concentrations higher than 15% (%w v^{-1}) corresponding to higher fibre dimension samples. These data suggested that an increase of the fibre dimensions resulted in a decrease of the density of the scaffolds, due to a lower packing degree of the thicker fibres. Based on these results, the solution concentration was fixed at 15% (% w v^{-1}) to allow fabrication of homogeneous and highly porous electrospun matrices.

The fibre diameter and the pore size distribution was also influenced by the flow rate (figures 3). At fixed values of solution concentration (15% w v^{-1}) and nozzle-collector distance (15 cm), fibre diameters significantly increased as the flow rate increased (respectively from 267±30 nm for G7_NF to 440±79 nm for G9_NF) since a higher flow rate caused a higher volume of spun solution, resulting in larger fibre dimensions. Furthermore, a flow rate of 10 µl min^{-1} was selected for fibre processing.

In order to examine the effect of electric field intensity on fibre morphology, four values of nozzle-collector distance (8, 10, 15 and 19 cm) were tested at fixed concentration of 15% and flow rate value of 10 µl min^{-1}.

As the nozzle-collector distance was increased, a significant (*$p<0.05$) reduction in the fibre diameters and their standard deviations was observed (figure 4(b)) and a more uniform fibre size distribution was obtained (figures 1 (d), (j), (k) and (l)) from 448±113 nm for G10_NF to 327±30 nm for G12_NF. Moreover, the pore dimension was slightly affected by the nozzle-collector distance (figures 4(a) and (c)) from 1.98±0.70 µm for G10_NF to 1.60±0.33 µm for G12_NF, showing no significant differences. In general high nozzle-collector

distances were preferred for nanofibres preparation to fabricate homogeneous 3D matrices. In details, a higher value of nozzle-collector distance induced a decrease in the electric field intensity, through which the fibres were produced. Moreover, the increase in the value of nozzle-collector distance involved two effects on the quality of fibres:

- increased time-of-flight and thus increase of the amount of solvent evaporated, reducing the formation of ribbon-like fibres;
- decreased force of attraction and tensions on the Taylor cone, which implied a greater uniformity of the jet. This induced a lower formation of beads and other surface defects.

3.2. Characterization of γ-glycidoxypropyltrimethoxysilane crosslinked nanofibres

3.2.1. Morphology and pore size. GL/GPTMS_NF were electrospun using the same spinning parameters as for G4_NF (paragraph 2.1.2). A solution concentration of 15% $w \cdot v^{-1}$, a flow rate of 10 $\mu l \cdot min^{-1}$ and a nozzle-collector distance of 15 cm were used. The morphology of electrospun mats was not significantly affected by the presence of the GPTMS crosslinker (figure 5 (a) and (b)) and the fibre and pore dimensions were respectively 327±45 nm and 1.64±0.37 μm, comparable to those of G4_NF (paragraph 3.1).

3.2.2. *Fourier transform infrared-attenuated total reflectance spectroscopy (FTIR-ATR).*

In Figure 5 (c), the FTIR-ATR spectra of GL_NF and GL/GPTMS_NF are reported. The two spectra showed the characteristic bands of the amide I, amide II and amide III, respectively at 1629 cm^{-1}, 1538 cm^{-1} and 1238 cm^{-1} for amide C=O stretching vibrations (amide I), amide N-H bending vibrations (amide II) and C–N stretching coupled with N–H in-plane bending vibrations (amide III) [43]. The GL_GPTMS FTIR-ATR spectrum showed a band at 920 cm^{-1} due to the stretching of Si-OH formed, by the hydrolysis of the trimethoxy groups of GPTMS during the crosslinking process. Moreover, the characteristic bands of Si–O–Si were observed at 1020 cm^{-1} and 1150 cm^{-1}, confirming the successful GPTMS crosslinking of GL [34].

3.2.3. Dissolution tests.

A qualitative analysis of the dissolution behaviour of GL/GPTMS_NF in PBS at 37°C confirmed the efficiency of the crosslinking process. After 6 hours incubation in PBS, the GL_NF were completely dissolved (figure 6 (d)) while the GL/GPTMS_NF preserved a fibrous morphology after 6 and 48 hours incubation in PBS (figure 6 (a) and (b)). After 168 hours, GL/GPTMS_NF samples showed a compact morphology (figure 6(c)), due to nanofibres swelling in PBS, followed by nanofibres collapse during nanofibres drying. Reported images are exemplary of the qualitative observation of sample morphology as a function of incubation time in PBS, as derived from the analysis of 5 samples per incubation time.

Moreover, quantitative measurements of weight loss were performed on GL/GPTMS_NF nanofibres (table 2).

Table 2. GL/GPTMS_NF nanofibres dissolution tests.

Time (days)	**Weight Loss average value ± standard deviation (%)**
1	7.58±0.3
2	11.55±0.77
4	18.98±0.37
7	29.45±1.51
10	46.14±3.54
14	77.14±2.56

3.2.4. In vitro cell test

Viability test: Adhesion and Proliferation assay

Adhesion and Proliferation assay.

The ability of the GL/GPTMS_NF to allow cell adhesion was verified by culturing NOBECs on both GL/GPTMS_NF and poly-L-lysine coated coverslips (control conditions). To determine the number of adherent cells, all nuclei with normal morphology were counted. The number of adherent cells counted after three hours of culture was expressed as the number of cells·mm^{-2}. Figure 7 (k) showed the number of

NOBECs which adhered after three hours, counted on GL/GPTMS_NF and poly-L-lysine coated coverslips, respectively. The number of adherent cells on GL/GPTMS_NF was statistical higher than in control conditions (*$p<0.05$).

NOBECs were seeded on GL/GPTMS_NF or poly-L-lysine coated coverslips and counted after 1, 3, 5 and 7 days. Figure 7(l) showed that no significant differences in cell numbers were observed in these two culture conditions. These data provided quantitative information about cell viability and adhesion, as well as their active proliferation on both GL/GPTMS_NF and in control conditions.

Apoptosis assay.

To detect and quantify apoptosis of cells seeded on GL/GPTMS_NF compared to control conditions, Tunel assay was performed as described above in the methods section. The Dead-End Fluorimetric Tunel system measures the fragmented DNA of apoptotic cells by catalytically incorporating fluorescein-12-dUTP at 3'-OH DNA ends using the Terminal Deoxynucleotidyl Transferase Recombinant enzyme (rTdT). rTdT forms a polymeric tail using the principle of the TUNEL (TdT-mediated dUTP Nick-End Labelling) assay. NOBECs were seeded on both GL/GPTMS_NF and in control conditions. Figure 8 showed apoptotic nuclei stained with DAPI (i and k) and Tunel (j and l) of NOBECs after treatment with 100 μM cycloheximide. In both DAPI and Tunel staining, nuclei appear pyknotic, due to the irreversible condensation of chromatin.

Few apoptotic nuclei were observed on GL/GPTMS_NF or in control conditions providing confirmation of the viability of the cells cultured on GL/GPTMS_NF (figure 8 (n) and (p)).

Figure 8(q) showed the percentage of apoptotic NOBECs counted on GL/GPTMS_NF and poly-L-lysine coated coverslips, respectively. There is no statistical difference between the percentage of apoptotic cells on GL/GPTMS_NF and control conditions (*$p<0.05$).

Moreover, NOBECs display a different distribution on GL/GPTMS_NF forming aligned clusters of cells (9 (c), (g), (k) and (o)) compared to the control condition in which they were randomly distributed (9 (a), (e), (f) and (m)).

Few apoptotic cells were observed on GL/GPTMS_NF as well as in the control conditions providing confirmation on the viability of the cells cultured on GL/GPTMS_NF (figure 8).

Figure 8 (q) showed the percentage of apoptotic NOBECs counted respectively on GL/GPTMS_NF and poly-L-lysine coating coverslips. There is no statistical difference between the percentage of apoptotic cells on GL/GPTMS_NF and control condition (*$p<0.05$).

Cell viability and cytotoxicity assay: 3-(4,5-dimethylthiazol-2-yl)-2,5-diphenyltetrazolium bromide (MTT) assay.

MTT assay was performed on NOBECs plated on both GL/GPTMS_NF and control condition in order to evaluate cell viability, cell proliferation, and potential GL nanofibres cytotoxicity. Treatment of cells with MTT results in a dark blue formazan product generated through the reduction of MTT by mitochondrial dehydrogenases in living cells. The MTT assay showed that absorbance value increased during 1 to 7 days confirming cell viability and the cell growth reported in the proliferation assay (figure 9). NOBECs displayed cellular viability on GL/GPTMS_NF and no statistical significance difference were observed compared to control condition at different time points. These results confirmed the non cytotoxicity of GL/GPTMS_NF that allowed cellular proliferation and viability.

Actin cytoskeleton Staining.

The actin cytoskeleton is a highly dynamic network composed of actin polymers. The function of actin cytoskeleton is to mediate a variety of essential biological functions including intra and extracellular movement and structural support. Orientational distribution of actin filaments within a cell is, therefore, an important determinant of cellular shape adhesion and motility. To confirm the capability of NOBECs to adhere on GL/GPTMS_NF actin cytoskeleton staining was performed using TRITC-conjugated phalloidin. NOBECs displayed a spread morphology with actin polymers organized into a filamentous network (F-actin, the major constituent of microfilaments) on both GL/GPTMS_NF and control condition (figure 10). The presence of a F-actin network provided qualitative information about the NOBECs elongated morphology and viability on GL/GPTMS_NF (figure 10 (f)).

Confocal microscopy.

To analyse the cellular response to electrospun GL/GTPMS_NF, NOBECs-GFP were seeded on GL/GTPMS_NF or on poly-L-lysine coated coverslips and incubated in DMEM supplemented with 10% FBS. Cell morphologies and distributions of NOBECs-GFP on nanofibres were studied by both fluorescence and confocal microscopy. Representative fluorescence (figure 7 and 8) and confocal (figure 11) microscopy images of NOBECs-GFP cultured for 1 and 3 days *in vitro* on GL/GTPMS_NF revealed that cells were organized in cords and the cell bodies had an elongated appearance with their longitudinal axis parallel to each other. In contrast, NOBECs-GFP were randomly distributed on poly-L-lysine coated coverslips and formed a continuous layer after 7 days *in vitro* (figure 7 (e)). The nanostructured architecture of the nanofibrous matrices influenced cell morphology and allowed NOBECs orientation, which could have a role in the formation of bands of Büngner and axonal elongation *in vivo***.**

4. Discussion

A wide variety of fibrous matrices were developed for tissue engineering applications [1-6] since the structure of these matrices can be designed to have high porosity, high surface-to-volume ratio, and high pore interconnectivity, all physical properties which can promote cellular adhesion and proliferation.

In this work, GL was selected as water soluble, non-expensive and commercially available ECM-derived material. GL crosslinked nanofibres were produced by electrospinning using aqueous solution to avoid the risk of protein denaturation and degradation and toxicity that can occur in presence of toxic solvent residues. A preliminary analysis on electrospinning of GL nanofibres was carried out to optimize the process parameters (solution concentration, flow rate and nozzle-collector distance) in order to obtain highly porous and homogeneous fibres with diameters of around 300 nm that have been reported to maximize the glial cells adhesion and proliferation [4]. The fabricated nanofibrous matrices were characterised by a wide range of fibre diameters combined or not with pore and/or beads formation, mainly depending on the polymer solution concentration, the spin flow rate and nozzle-collector distance. The voltage applied to make the nanofibrous matrices was fixed to 30 kV and the solutions were electrospun at 50°C.

Highly concentrated solutions (20%) produced thick fibres while both beads and droplet formed at low concentrations (8%). Significant differences ($*p<0.05$) of fibre diameters were observed for samples

prepared from solution with 8%, 10%, 12% concentrations with respect to 20%. A more homogeneous distribution of fibre size was measured at intermediate concentrations (figure 2(b)) in the range of spinnability (from 8% to 20%).

Fibre size significantly increased (*$p<0.05$) by increasing the flow rate (figure 3(b)) even if beads morphologies appeared when the flow rate was too high (figure 1(i)).

The effect of the electric field intensity on fibre size was evaluated by varying the nozzle-collector distance. When the distance was increased, the fibre dimension significantly decreased (*$p<0.05$,figure 4(b)). On the other hand, no significant differences (*$p<0.05$) were observed for pore dimensions with respect to process parameters.

GL/GPTMS_NF were electrospun using an intermediate solution concentration (15%), a high nozzle-collector distance of 15 cm and a flow rate of 10 $\mu l \cdot min^{-1}$ were selected for the production of nanofibrous matrices.

Crosslinked GL nanofibres were prepared to ensure GL stability in an aqueous environment, such as biological fluids. GPTMS was selected as a biocompatible crosslinker and added to the GL solution before electrospinning. As previously described, GPTMS is advantageous for the electrospinning process as crosslinking occurs only after solvent evaporation [44] and not affected the fibre morphology as observed for other crosslinkers [28].

The GL/GPTMS_NF had fibre diameters and pore dimensions of 327±45 nm and 1.64±0.37 μm respectively (figure 5 (a) and (b)) and showed stability in an aqueous environment (figure 6 (a), (b) and (c)).

In this work, GL/GTPMS_NF were found to support the in vitro adhesion, proliferation and survival of NOBECs when compared to control conditions (figure 7, 8 and 9). Previous studies by the authors [45] reported a decrease in the number of MG63 osteoblast-like cells when seeded on GL/GPTMS microporous membranes due to their lower hydrophilicity compared to GL. On the other hand, the nanostructured texture of the GL/GTPMS_NF improved NOBECs adhesion and allowed NOBECs proliferation and viability. After 24 hours cultured, NOBECs showed a spread morphology and the presence of an actin filaments network was observed (figure 10) both on GL/GTPMS_NF and control condition. Moreover, fluorescence and confocal microscopy images of NOBECs-GFP on GL/GTPMS_NF revealed that cell bodies had an elongated appearance with their longitudinal axis parallel to each other (figure 11). In contrast, NOBEC-GFP

were randomly distributed in control conditions. This preliminary results suggested that structural features such as nanofibrous matrices and ECM-derived materials can offer suitable cues for the adhesion, proliferation and organization of glial cells after injuries allowing the formation of the bands of Büngner, crucial for the direction of axon growth [46].

5. Conclusion

This study illustrated the possibilities of fabricating GPTMS crosslinked GL nanofibres by electrospinning techniques avoiding the use of toxic solvents. The manipulation of the spinning parameters to tailor the fibre diameter was described. The suitability of the developed nanofibrous scaffolds as a substrate for glial cells growth was analized in terms of NOBECs cells viability and morphology. NOBECs-GFP on GL/GTPMS_NF revealed that cell bodies had an elongated appearance. The elongated morphology of cells should enhance the formation of a cable along which axons might regenerate *in vivo*. Moreover, the adhesion and proliferation of NOBECs on nanofibrous substrates might increase the gap that can be bridged by producing extracellular matrix molecules and growth factors.

Further investigations will be addressed to analyze the *in vivo* response of GL/GTPMS_NF, as internal fillers for hollow nerve guidance channels, to verify their ability to promote peripheral nerve regeneration.

Acknowledgment

This work was supported by the Regione Piemonte ("Bando Ricerca Sanitaria Finalizzata") and the Compagnia San Paolo (MOVAG Project). Chiara Tonda Turo's Grant is provided by CRT- Lagrange Project. A special thanks to Dr. Antonella Silvestri, Politecnico di Torino, for useful advices.

Caption to Figures

Figure 1. SEM micrographs of GL nanofibres varying solution and process parameters (solution concentration, flow rate, nozzle-collector distance).
(a) G1_NF (8%, 10 µl min^{-1},15 cm), (b) G2_NF (10%, 10 µl min^{-1},15 cm), (c) G3_NF (12%, 10 µl min^{-1},15 cm), (d) G4_NF (15%, 10 µl min^{-1},15 cm), (e) G5_NF (18%, 10 µl min^{-1},15 cm), (f) G6_NF (20%, 10 µl min^{-1},15 cm), (g) G7_NF (15%, 8 µl min^{-1},15 cm), (h) G8_NF(15%, 12 µl min^{-1},15 cm), (i) G9_NF (15%, 15 µl min^{-1},15 cm), (j) G10_NF (15%, 10 µl min^{-1},7 cm), (k) G11_NF (15%, 10 µl min^{-1},10 cm), (l) G12_NF (15%, 10 µl min^{-1},19 cm).

Figure 2. Morphological characteristics of GL nanofibres varying the GL solution concentration at a constant value of flow rate (10 µl min^{-1}) and nozzle-collector distance (15 cm): (a) pore size distribution, (b) fibre dimension and (c) pore diameter. Statistical analysis was carried out using one-way ANOVA (*$p<0.05$).

Figure 3. Morphological characteristics of GL nanofibres varying the flow rate at a constant value of solution concentration (15 % w v^{-1}) and nozzle-collector distance (15 cm): (a) pore size distribution, (b) fibre dimension and (c) pore diameter. Statistical analysis was carried out using one-way ANOVA (*$p<0.05$).

Figure 4. Morphological characteristics of GL nanofibres varying the nozzle-collector distance at a constant value of solution concentration (15 % w v^{-1}) and flow rate (10 µl min^{-1}): (a) pore size distribution, (b) fibre dimension and (c) pore diameter. Statistical analysis was carried out using one-way ANOVA (*$p<0.05$).

Figure 5. SEM micrograph of (a) GL4_NF and (b) GL/GPTMS_NF (bar 10µm). (c) GL4_NF and GL/GPTMS_NF FTIR_ATR spectra. Black arrows indicated the presence of Si-O-Si and Si-OH bonds.

Figure 6. Images and SEM micrograph (bars 10µm) of GL/GPTMS_NF after (a) 6, (b) 48 and (c) 168 hours immersion in PBS. (d) After 6 hours uncrosslinked nanofibres (G4_NF) were completely dissolved.

Figure 7. Viability test: Adhesion and Proliferation assay. Fluorescence image after nuclear DAPI staining of NOBECs seeded on (a-e) poly-L-lysine coated coverslips (control condition) and (f-j) GL/GPTMS_NF after (a, f) 3 hours (3h), (b, g) 1 day (1D), (c, h) 3 days (3D), (d, i) 5 days (5D) and (e, j) 7 days (7D). Scale bar: 100 µm. (k) Number of adherent cells after 3 hours expressed as cells mm^{-2} on GL/GPTMS_NF and control condition. (l) NOBECs proliferation ratio after 1, 3, 5, and 7 days on control condition and GL/GPTMS_NF substrates. No significant differences between GL/GPTMS_NF substrates and control were observed to any of the experimental times tested.

Figure 8. Apoptosis assay. Cells were stained with (a, e, i, m, c, g, k, o) DAPI and (b, f, j, n, d, h, l, p) TUNEL after starvation for 3 days in SFM and photographed under a fluorescence microscope. (b,d) Technical negative control preparing using a control incubation buffer without rTdT; (f,h) technical positive control using DNase I; (j,l) positive control for biological apoptosis performed by 24 h treatment with 100 µM CHX and (n,p) NOBECs after 3 days in SFM (3D SFM). Scale bar 100 µm. (q) The percentage of apoptotic nuclei stained with TUNEL/total nuclei stained with DAPI was calculated from four arbitrary fields.

Figure 9. Cell viability and cytotoxicity assay: 3-(4,5-dimethylthiazol-2-yl)-2,5-diphenyltetrazolium bromide (MTT) assay. At 1, 3, 5, 7 days in culture cells were analyzed for viability by MTT assay. The absorbance value measured at 570 nm on control condition and GL/GPTMS_NF is represented (A). The number of cell, at the different time points, on GL/GPTMS_NF compare to control condition was calculated by normalizing absorbance value to a calibration curve (B). Viability percentage (relative to control condition) is reported (C).

Figure 10. Actin cytoskeleton Staining. NOBEC cells were plated on control condition (A, B, C) and GL/GPTMS_NF (D, E, F). After 24 h TRITC conjugated phalloidin was performed and pictures were taken

at low magnification with a Plan Fluor 20× (Nikon) (numerical aperture (NA) = 0.45) (A, B, D and E) and at a high magnification with Plan Fluor 40× (Nikon) (numerical aperture (NA) = 0.75) (C and F).

Figure 11. Confocal microscopy images of NOBECs-GFP (b, f, d, h) and after nuclear staining (a, e, c, g) cultured for (a, b, e, f) 1 day and (c, d, g, h) 3 day on GL/GPTMS_NF. Scale bar: 50 μm.

References

[1] S. Agarwal, J.H. Wendorff, A. Greiner, Use of electrospinning technique for biomedical applications, Polymer 49 (2008) 5603-5621

[2] H.S. Koh, T. Yong, C.K. Chan, S. Ramakrishna, Enhancement of neurite outgrowth using nano-structured scaffolds coupled with laminin, Biomaterials 29 (26) (2008) 3574-3582

[3] V. Mahairaki, S.H. Lim, G.T. Christopherson, L. Xu, I. Nasonkin, C. Yu, H.Q. Mao, V.E. Koliatsos, Nanofiber Matrices Promote the Neuronal Differentiation of Human Embryonic Stem Cell-Derived Neural Precursors *In Vitro*, Tissue Eng. Part A 17(5-6) (2011) 855-863

[4] G.T. Christopherson, H. Song, H.Q. Mao, The influence of fiber diameter of electrospun substrates on neural stem cell differentiation and proliferation, Biomaterials 30 (2009) 556–564

[5] F. Yang, R. Murugan, S. Wang, S. Ramakrishna, Electrospinning of nano/micro scale poly(L-lactic acid) aligned fibers and their potential in neural tissue engineering, Biomaterials 26 (2005) 2603–2610.

[6] M.B. Steed, V. Mukhatyar, C. Valmikinathan, R.V. Bellamkonda, Advances in Bioengineered Conduits for Peripheral Nerve Regeneration, Atlas Oral Maxillofacial Surg. Clin. N. Am. **19** (2011) 119–130

[7] C. Xu, F. Yang, S. Wang, S. Ramakrishna, *In vitro* study of human vascular endothelial cell function on materials with various surface roughness, J. Biomed. Res. Part A 71A (2004) 154–161

[8]T.B. Bini, S. Gao, S. Wang, S. Ramakrishna, Poly(l-lactide-co-glycolide) biodegradable microfibers and electrospun nanofibers for nerve tissue engineering: an *in vitro* study, J. Mater. Sci. 41(19) (2006) 6453–6459

[9] S. A. Riboldi, M. Sampaolesi, P. Neuenschwander, G. Cossu, S. Mantero, Electrospun degradable polyesterurethane membranes: potential scaffolds for skeletal muscle tissue engineering, Biomaterials 26 (2005) 4606–4615

[10] P. C. Caracciolo, V. Thomas, Y. K. Vohra, F. Buffa, G.A. Abraham, Electrospinning of novel biodegradable poly(ester urethane)s and poly(ester urethane urea)s for soft tissue-engineering applications, J. Mater. Sci.: Mater. Med. 20 (2009) 2129–2137.

[11]L. Ghasemi-Mobarakeh, M.P. Prabhakaran, M. Morshed, M.H. Nasr-Esfahani, S. Ramakrishna, Electrospun poly(ε -caprolactone)/gelatin nanofibrous scaffolds for nerve tissue engineering, Biomaterials 29 (2008) 4532–4539

[12] M.D. Schofer, U. Boudriot, I. Leifeld, R.I. Sütterlin, M. Rudisile, J.H. Wendorff, A. Greiner, J.R.J. Paletta, S. Fuchs-Winkelmann, Characterization of a PLLA-collagen blend nanofiber scaffold with respect to growth and osteogenic differentiation of human mesenchymal stem cells, ScientificWorldJournal 9 (2009) 118–129

[13] P. C. Caracciolo, V. Thomas, Y. K. Vohra, F. Buffa, G.A. Abraham, Elect
rospinning of novel biodegradable poly(ester urethane)s and poly(ester urethane urea)s for soft tissue-engineering applications, J. Mater. Sci.: Mater. Med. 20 (2009) 2129–2137.

[14]L. Ghasemi-Mobarakeh, M.P. Prabhakaran, M. Morshed, M.H. Nasr-Esfahani, S. Ramakrishna, Electrospun poly(ε -caprolactone)/gelatin nanofibrous scaffolds for nerve tissue engineering, Biomaterials 29 (2008) 4532–4539

[15] H. Homayoni, S. Hosseini Ravandi, M. Valizadeh, Electrospinning of chitosan nanofibers: Processing optimization, Carbohyd. Polym. **77** (2009) 656–661

[16] K.S. Rho, L. Jeong, G. Lee, B.M. Seo, Y.J. Park, S.D. Hong, S. Roh, J. Jae Cho, W.H. Park, B.M. Min, Electrospinning of collagen nanofibers: Effects on the behavior of normal human keratinocytes and early-stage wound healing, Biomaterials 27 (2006) 1452–1461

[17] S. Torres-Giner, J. V. Gimeno-Alcantiz, M. J. Ocio, J.M. Lagaron, Comparative performance of electrospun collagen nanofibers cross-linked by means of different methods, Appl. Mater. Interfaces 1 (1) (2009) 218-223
[18] C. Tonda-Turo, C. Audisio, S. Gnavi, V. Chiono, P. Gentile, S. Raimondo, S. Geuna, I. Perroteau, G. Ciardelli, Porous poly(ε -caprolactone) nerve guide filled with porous gelatin matrix for nerve tissue engineering, Adv. Eng. Mater. 13(5) (2011) B151-B164
[19] G. Ciardelli, P. Gentile, V. Chiono, M. Mattioli-Belmonte, G. Vozzi, N. Barbani, P. Giusti, Enzymatically crosslinked porous composite matrices for bone tissue regeneration, J. Biomed. Mater. Res. Part A 92A (2009) 137–151
[20] V. Chiono, E. Pulieri, G. Vozzi, G. Ciardelli, A. Ahluwalia, P. Giusti, Genipin-crosslinked chitosan/gelatin blends for biomedical applications, J. Mater. Sci: Mater. Med. 19 (2008) 889-898
[21] Z.M. Huang, Y.Z. Zhang, S. Ramakrishna, C. T. Lim, Electrospinning and mechanical characterization of gelatin nanofibres, Polymer 45 (2004) 5361–5368
[22] J.H. Song, H.E. Kim, H.W. Kim, Production of electrospun gelatin nanofiber by water-based co-solvent approach, J. Mater. Sci. Mater. Med. 19 (2008) 95–102
[23] H.W. Kim, J.H. Song, H.E. Kim, Nanofiber generation of gelatinhydroxyapatite biomimetics for guided tissue regeneration, Adv. Funct. Mater. 15 (2005) 1988–1994
[24] C.S. Ki, D.H. Baek, K.D. Gang, K.H. Lee, I.C. Um, Y.H. Park, Characterization of gelatin nanofiber prepared from gelatin-formic acid solution, Polymer 46 (2005) 5094–5102
[25] G.A. Digenis, T.B. Gold, V.P. Shah, Cross-linking of gelatin capsules and its relevance to their *in vitro-in vivo* performance, Pharm. Sci. 83 (1994) 915–921
[26] A.J. Kuijpers, G.H.M. Engbers, J. Krijgsveld, S.A.J. Zaat, J. Dankert, J.Feijen, , Cross-linking and characterisation of gelatin matrices for biomedical applications, J. Biomater. Sci. Polym. Ed. 11 (2000) 225–243
[27] Y.Z. Zhang, J. Venugopal, Z.M. Huang, C.T. Lim, S. Ramakrishna, Crosslinking of the electrospun gelatin nanofibres, Polymer 47 (8) (2006) 2911–2917
[28] S. Panzavolta, M. Gioffrè, M. L. Focarete, C. Gualandi, L. Foroni, A. Bigi, Electrospun gelatin nanofibers: Optimization of genipin cross-linking to preserve fiber morphology after exposure to water, Acta Biomat. 7 (2011) 1702–1709
[29] S. Zhang, Y. Huang, X. Yang, F. Mei, Q. Ma, G. Chen, S. Ryu, X. Deng, Gelatin nanofibrous membrane fabricated by electrospinning of aqueous gelatin solution for guided tissue regeneration, J. Biomed. Mater. Res. 90A (2009) 671–679
[30] L. Ma, C. Gao, Z. Mao, J. Shen, X. Hu, C. Han, Thermal dehydration treatment and glutaraldehyde cross-linking to increase the biostability of collagen-chitosan porous scaffolds used as dermal equivalent, Biomater. Sci. Polym. Ed. 14 (2003) 861–874
[31] H. Ueda, T. Nakamura, M. Yamamoto, N. Nagata, S. Fukuda, Y. Tabata, Y. Shimizu, Repairing of rabbit skull defect by dehydrothermally crosslinked collagen sponges incorporating transforming growth factor β1, J. Control. Release 88 (2000) 55–64
[32] E.E. Delyth, F.J. Davis, G.R. Mitchell, R.H. Olley, Structure development in electrospun fibres of gelatin, Journal of Physics (2009) Conf.Series 183 012021
[33] O. Mahony, O. Tsigkou, C. Ionescu, C. Minelli, L. Ling, R. Hanly, M.E. Smith, M.M. Stevens, J.R. Jones, Silica-Gelatin Hybrids with Tailorable Degradation and Mechanical Properties for Tissue Regeneration, Adv. Func. Mat. 20 (22) (2010) 3835–3845
[34] A.C. Chao, Preparation of porous chitosan/GPTMS hybrid membrane and its application in affinity sorption for tyrosinase purification with Agaricus bisporus, J. Mem. Sci., 311 (2008) 306–318
[35] K. Wewetzer, E. Verdu, D.N. Angelov, X. Navarro, Olfactory ensheathing glia and Schwann cells; two of a kind?, Cell Tissue Res. 309 (2002) 337–345
[36] L. L. Jones, R.U. Margolis, M.H. Tuszynski, The chondroitin sulfate proteoglycans neurocan, brevican, phosphacan and versican are differentially regulated following spinal cord injury, Exp. Neurol. 182 (2003) 399–411
[37]M. Agudo, A. Woodhoo, D. Webber, R. Mirsky, K.R. Jessen, S.B. McMahon, Schwann cell precursors transplanted into the injured spinal cord multiply, integrate and are permissive for axon growth, Glia 56 (12) (2008) 1263–1270

[38] You, H. Wei, L. Liu, Y. Oudega, M. Jiao, S.S. Feng, S.N. Chen, Y. Chen, J.M. Li, B.C., Olfactory ensheathing cells enhance Schwann cell-mediated anatomical and functional repair after sciatic nerve injury in adult rats, Exp Neurol. 229(1) (2011) 158-67.
[39] T.J. Sill, H.A. von Recum, Electrospinning: Applications in drug delivery and tissue engineering, Biomaterials 29 (2008) 1989-2006
[40] Y.L. Liu, Y.H. Su, J.Y. Lai, Preparation and characterization of a chitosan–silica hybrid membrane, Polymer 45 (2004) 6831–6837
[41] M.N. Goodman, J. Silver, J.W. Jacobberger, Establishment and neurite outgrowth properties of neonatal and adult rat olfactory bulb glial cell lines, Brain Res. 619 (1993) 199-213
[42] X. Liu, J.M. Yang, S.S. Zhang, X.Y. Liu, D.X. Liu, Induction of cell cycle arrest at G1 and S phases and cAMP-dependent differentiation in C6 glioma by low concentration of cycloheximide, BMC Cancer 10 (2010) 684-692
[43] J.H. Muyonga, C.G.B. Cole, K.G. Duodu, Extraction and physico- chemical characterization of Nile perch (Lates niloticus) skin and bone gelatin, Food Chem. 86 (2004) 325–332.
[44] K. Sisson, C. Zhang, M.C. Farach-Carson, D.B. Chase, J.F. Rabolt, Evaluation of crosslinking methods for electrospun gelatin on cell growth and viability, Biomacromol. 10 (2009) 1675–1680
[45] C. Tonda-Turo, P. Gentile, S. Saracino, V. Chiono, V. K. Nandagiri, G. Muzio, R.A. Canuto, G. Ciardelli, Comparative analysis of gelatin scaffolds crosslinked by genipin and silane coupling agent, Int. J. Biol.Macromol. 49 (4) (2011) 700-706
[46]R. Deumens, A. Bozkurt, M. F. Meek, M. A. E. Marcus, E.A.J. Joosten, J. Weis, G.A. Brook, Repairing injured peripheral nerves: Bridging the gap, Prog. Neurobiol. 92 (2010) 245–276

Figure 1

Click here to download high resolution image

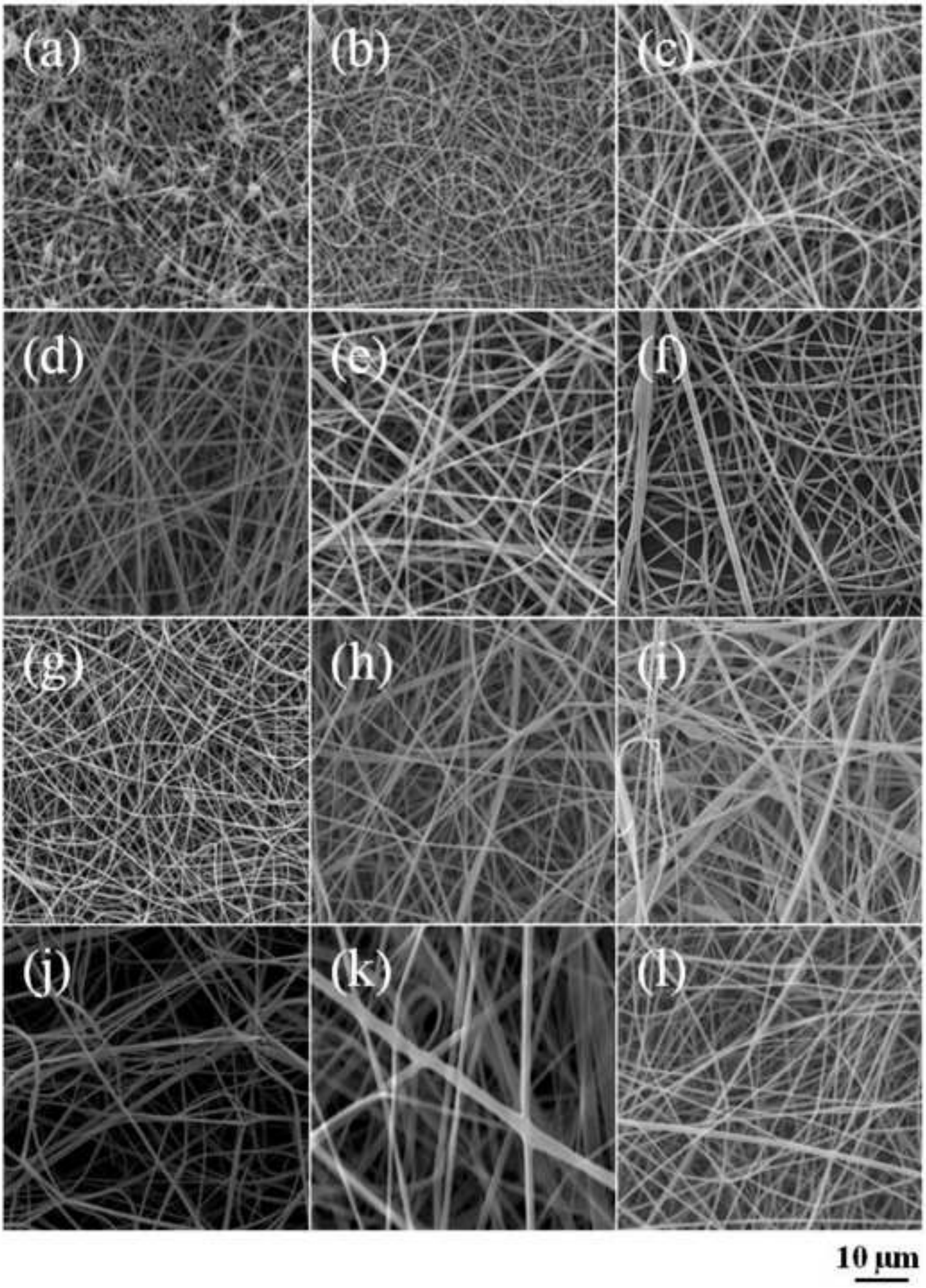

Figure 2

Click here to download high resolution image

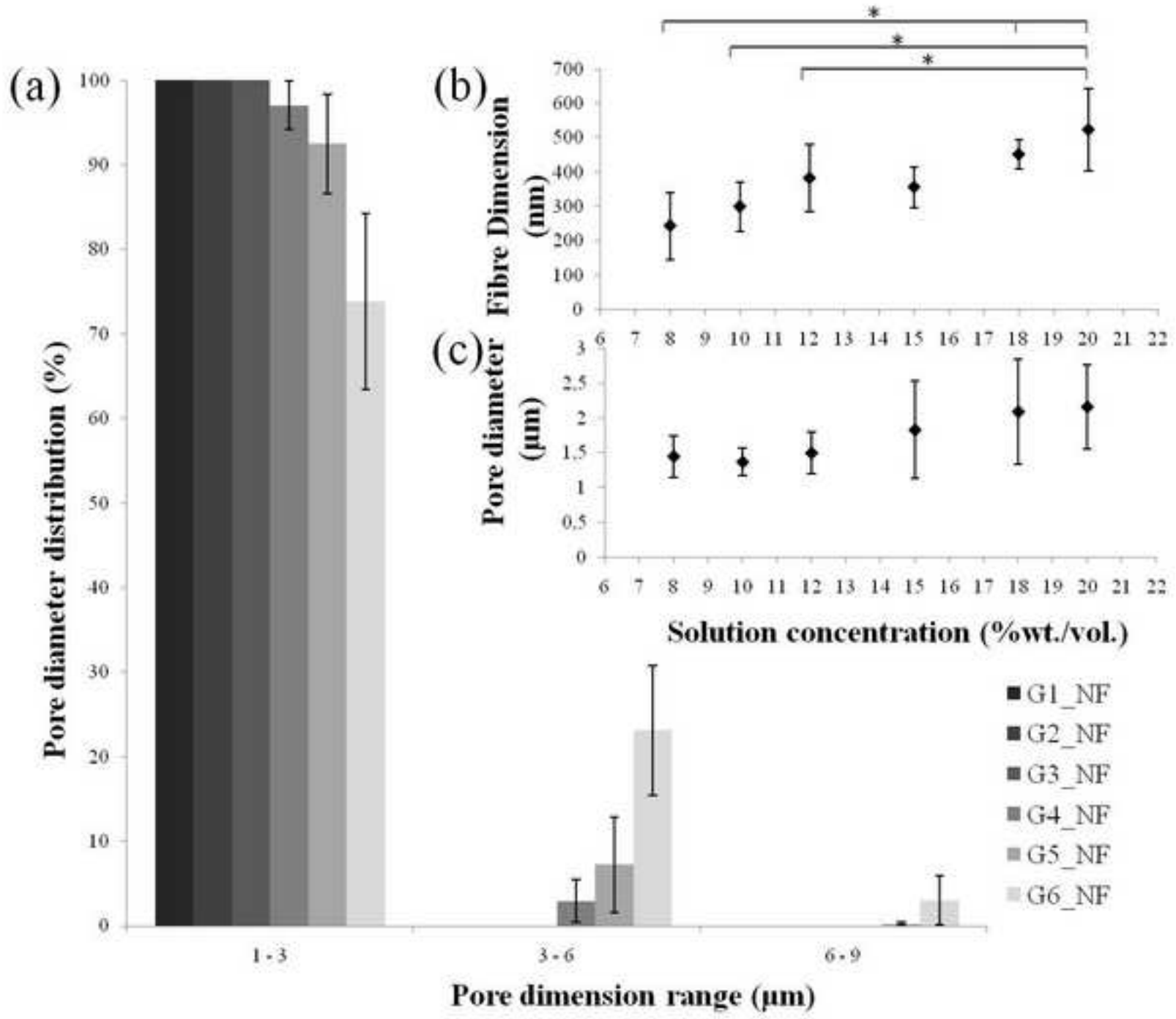

Figure 3

Click here to download high resolution image

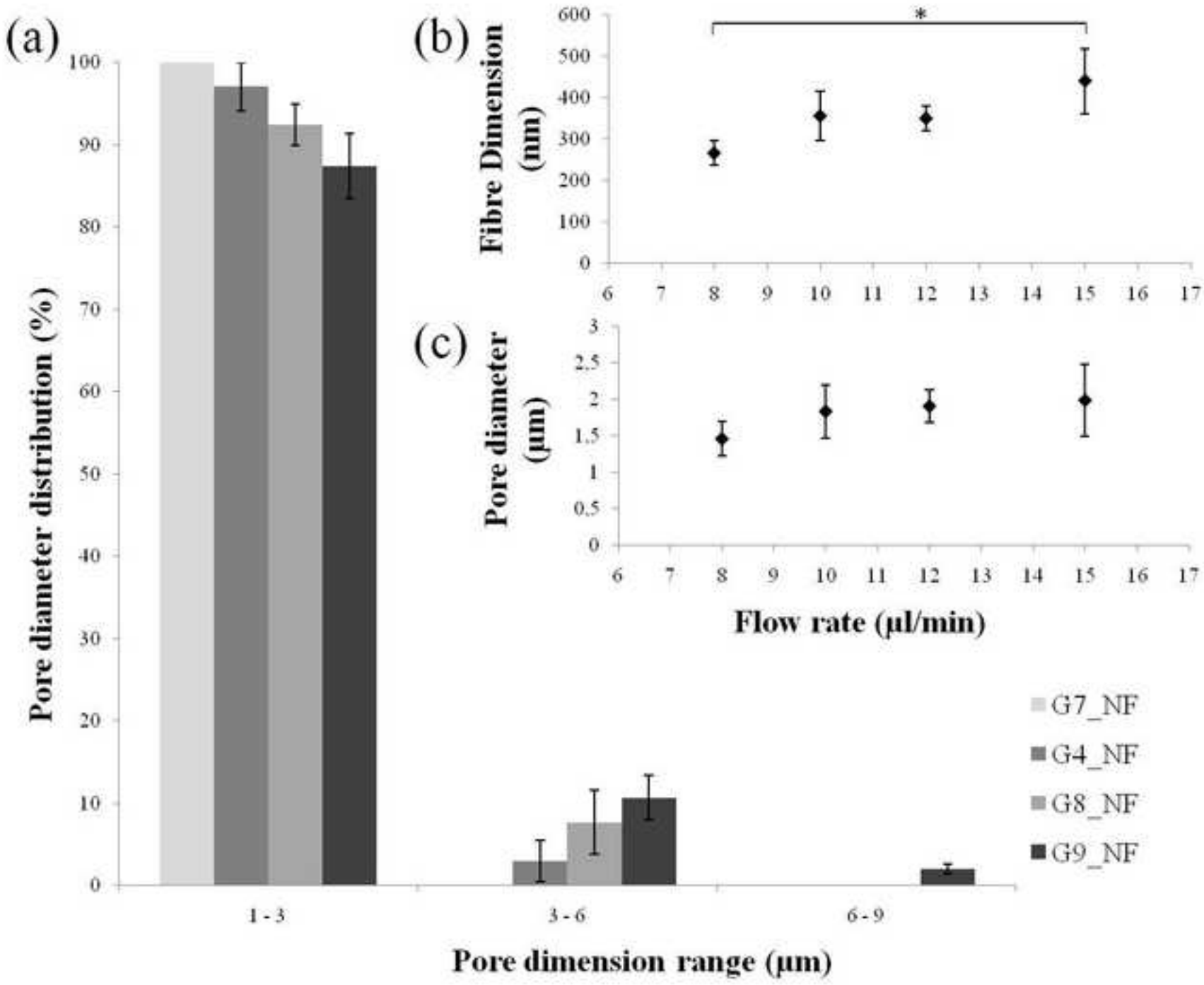

Figure 4

Click here to download high resolution image

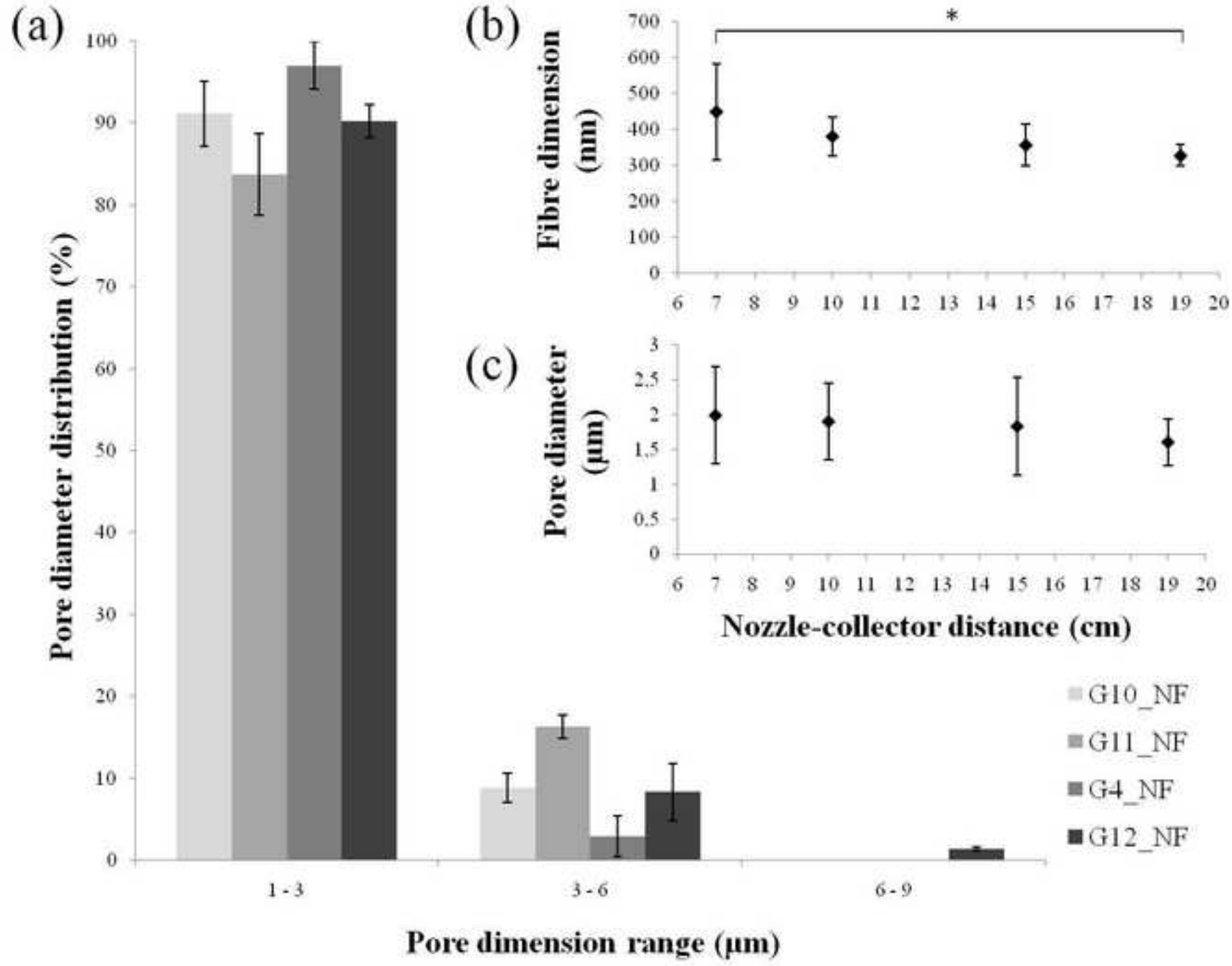

Figure 5

Click here to download high resolution image

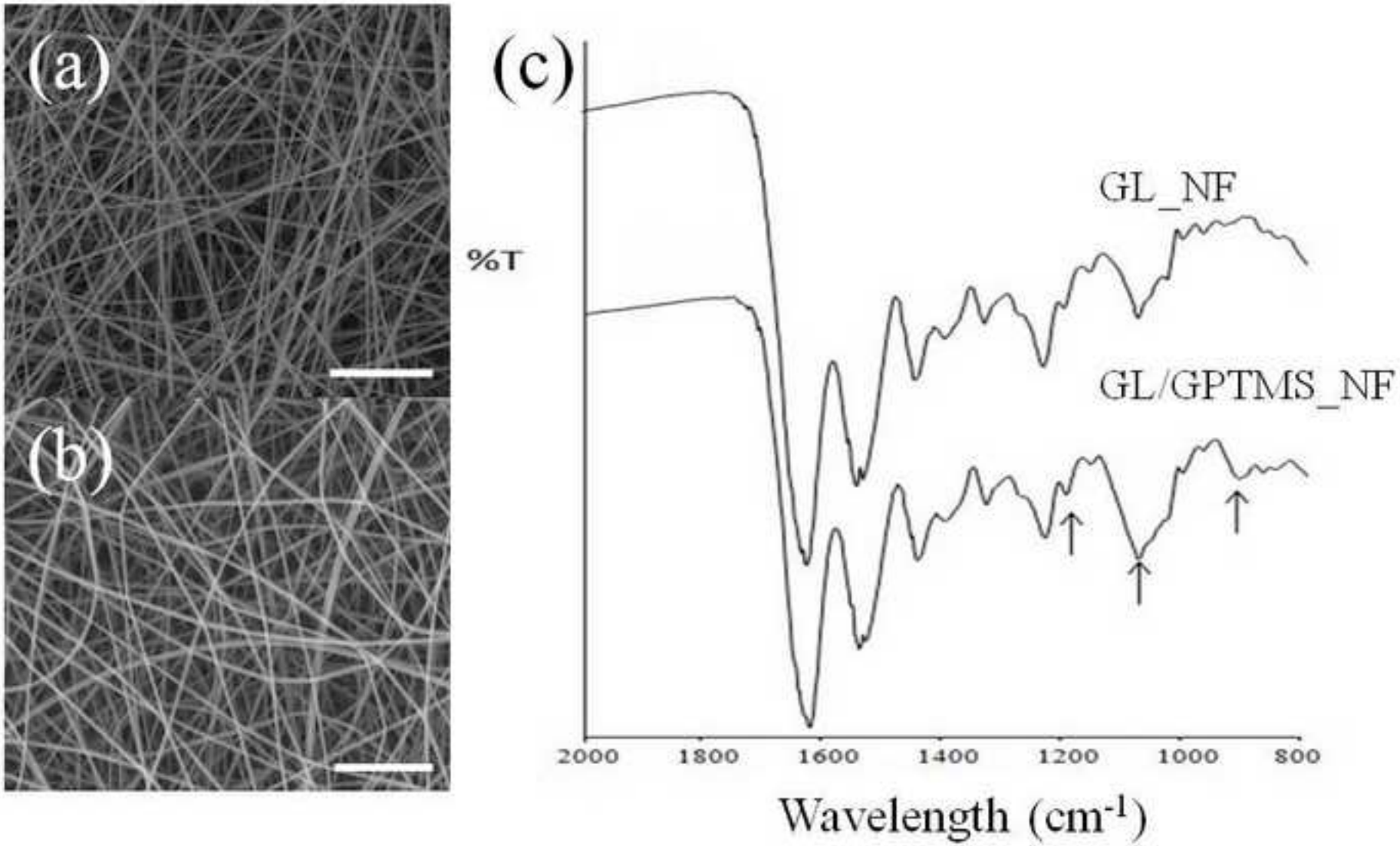

Figure 6

Click here to download high resolution image

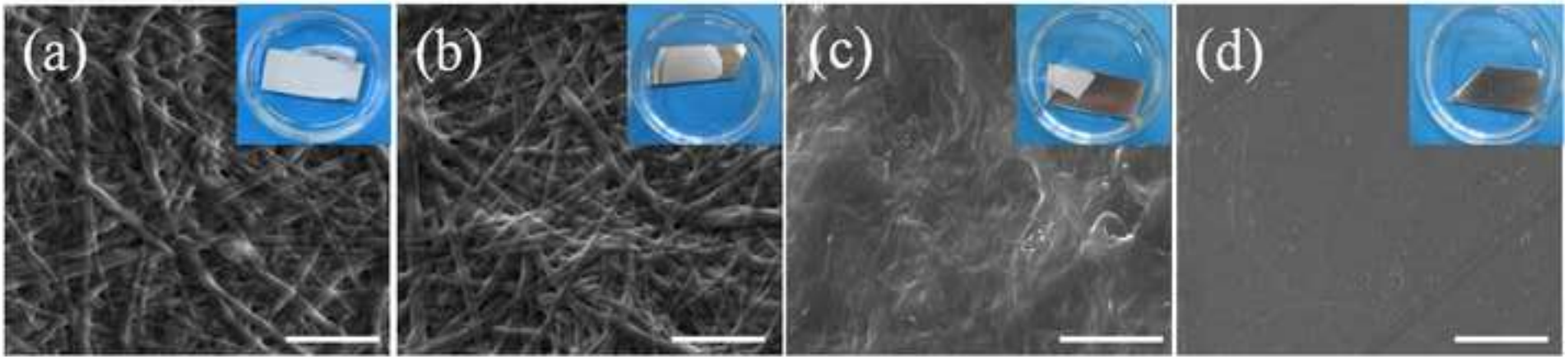

Figure 7

Click here to download high resolution image

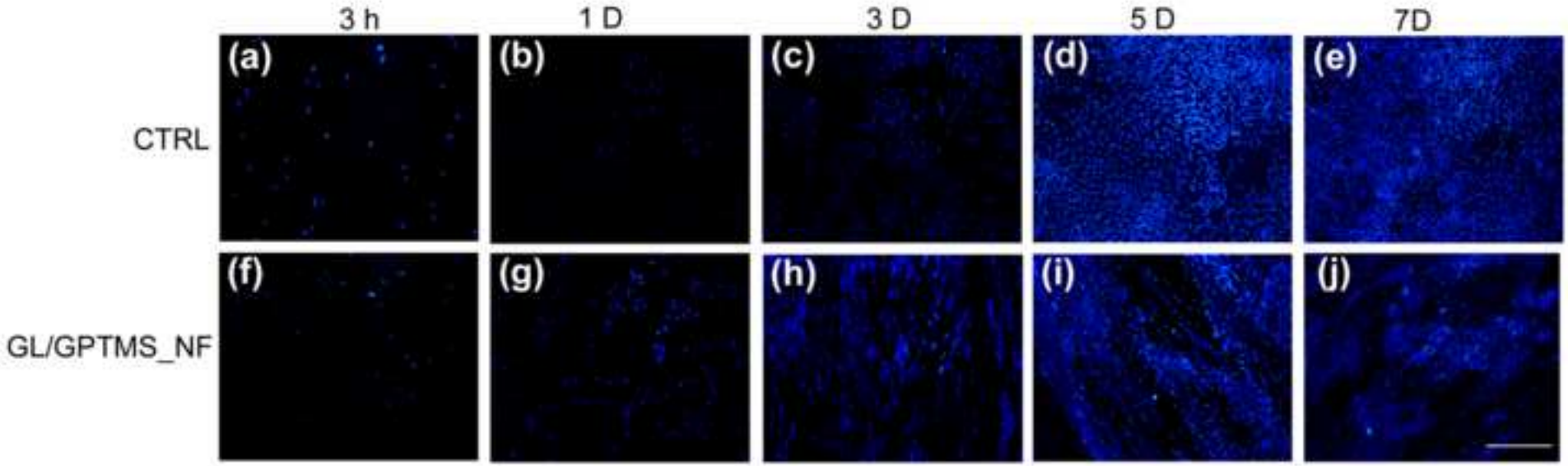

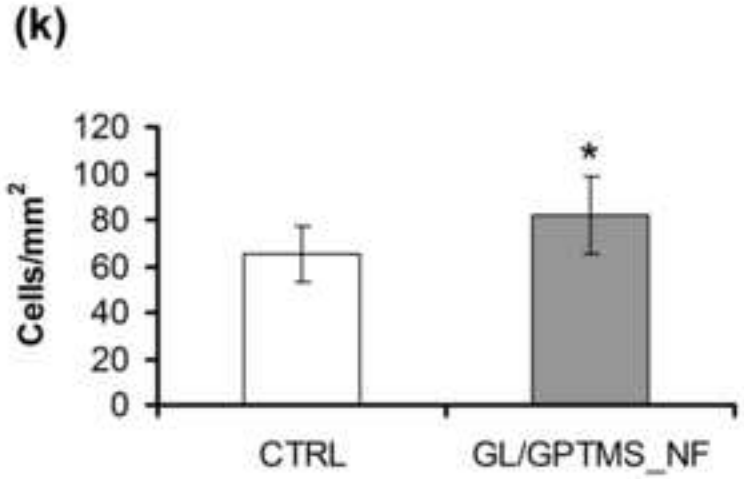

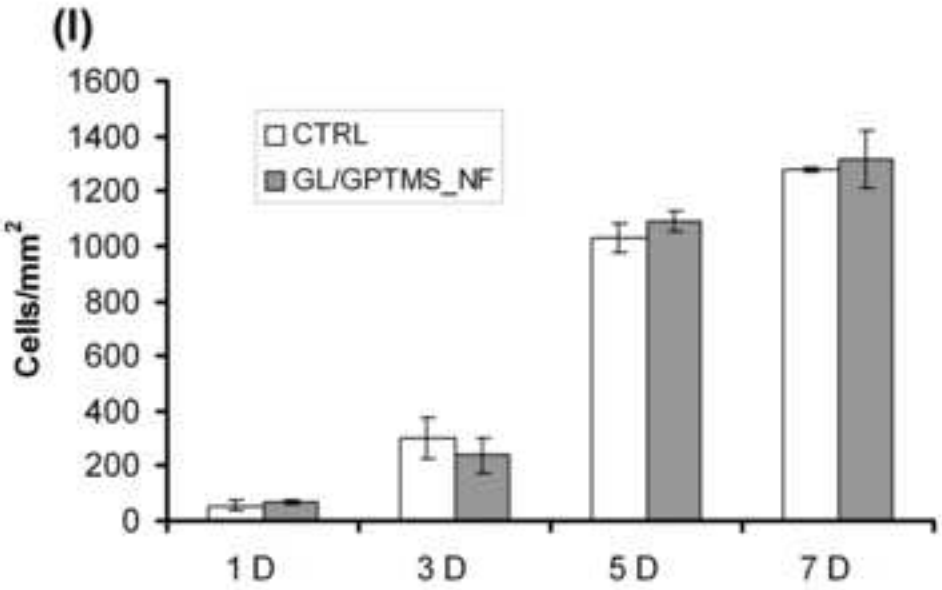

Figure 8

Click here to download high resolution image

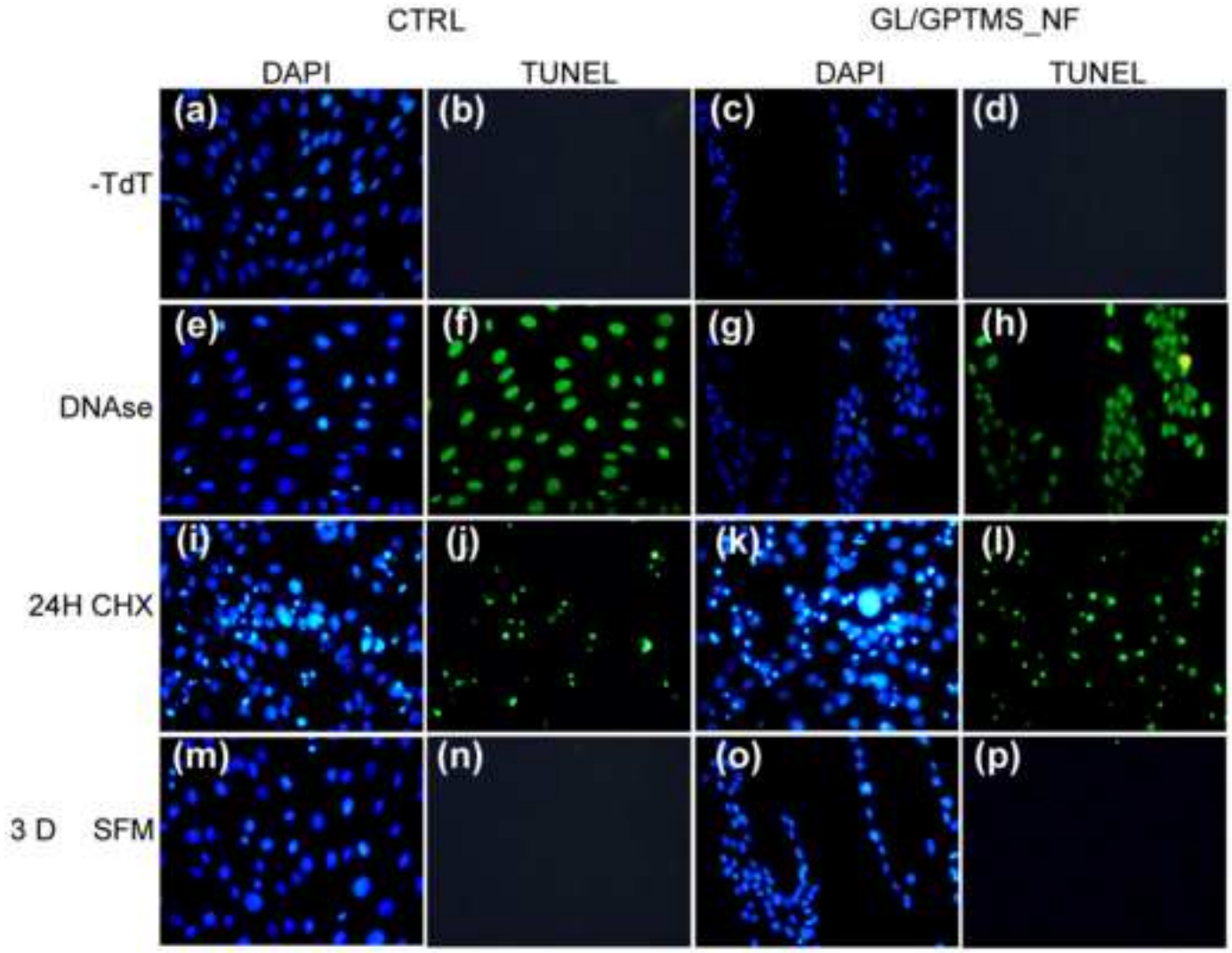

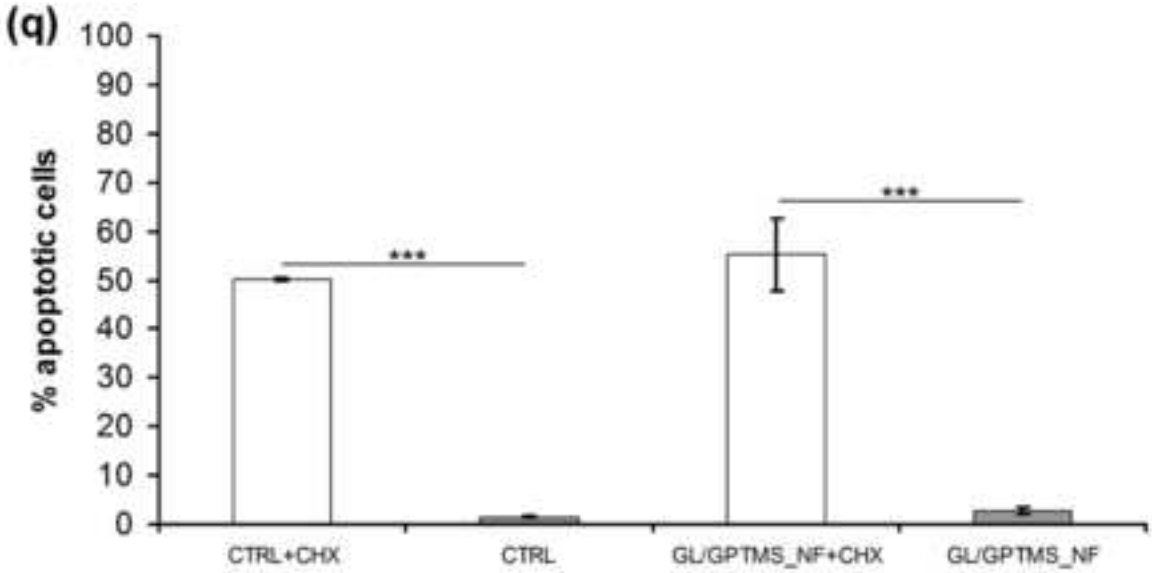

Figure 9

Click here to download high resolution image

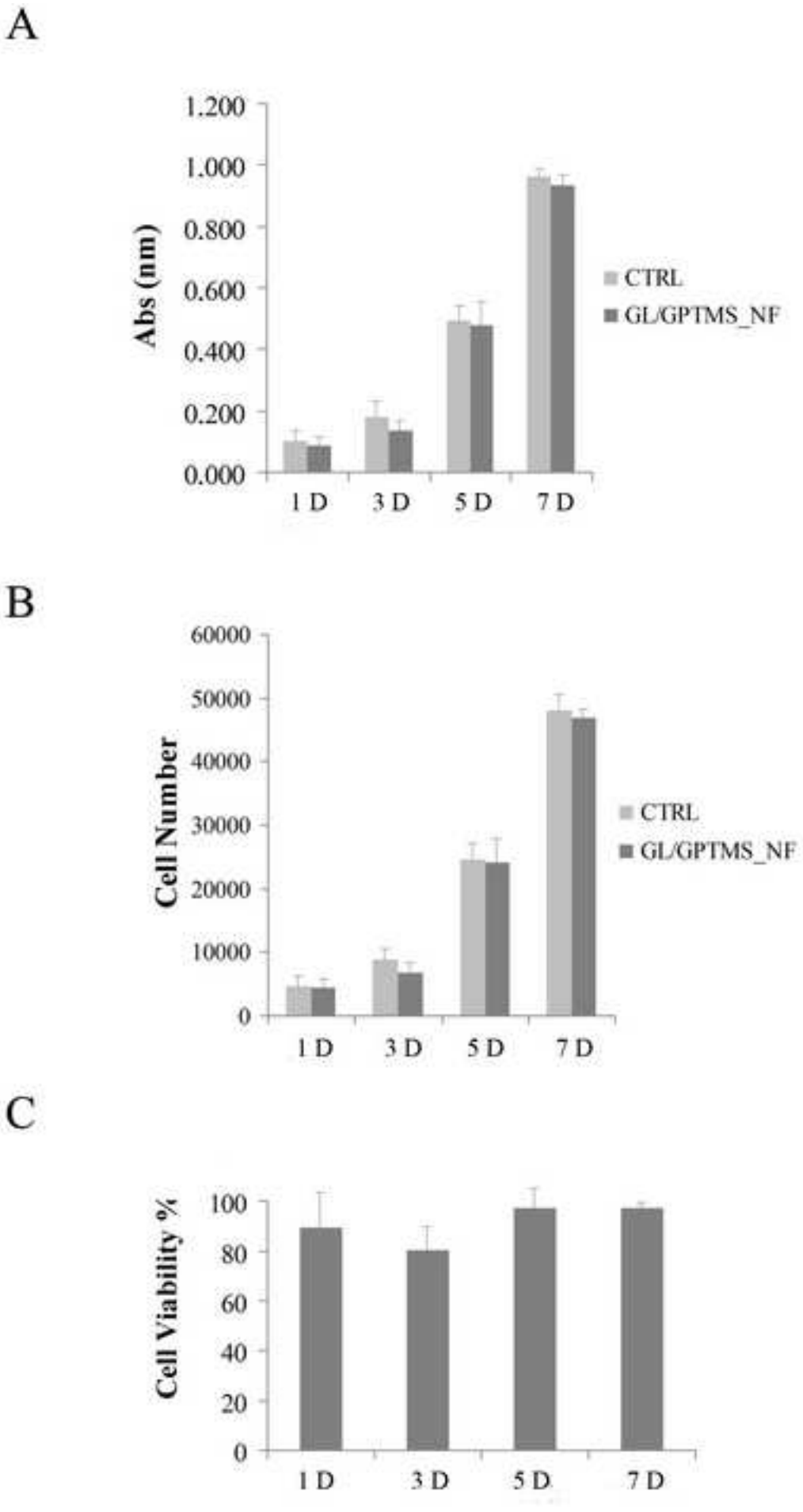

Figure 10

Click here to download high resolution image

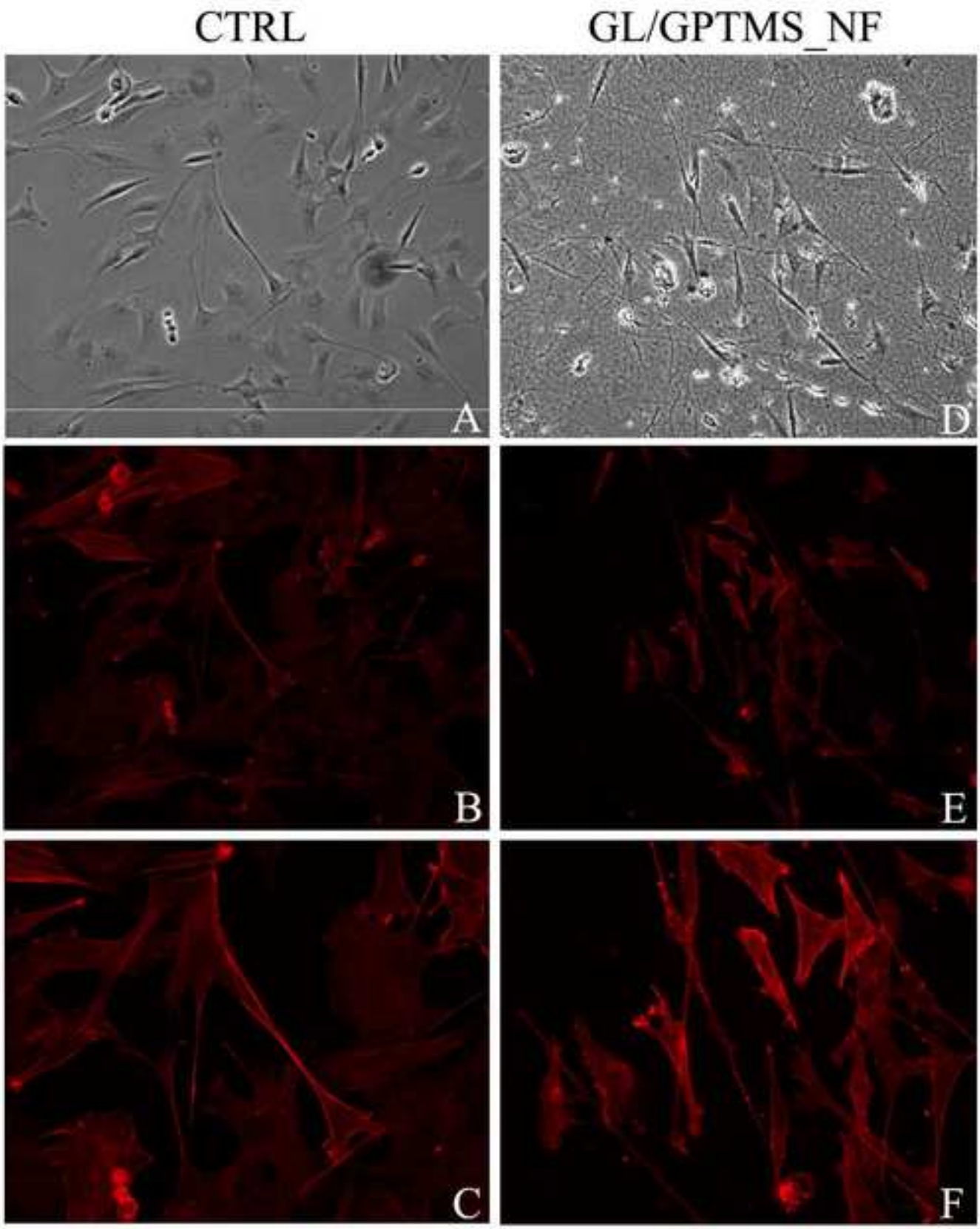

Figure 11

Click here to download high resolution image